Water transport control on a patterned superhydrophobic surface via laser direct writing

Tianchi Chen
College of Mechanical and Electrical Engineering, China University of Mining and Technology, Xuzhou 221116, China

Hongtao Liu,[a] Shuhua Teng, and Wei Yan
College of Materials Science and Engineering, China University of Mining and Technology, Xuzhou 221116, China

Haifeng Yang
College of Mechanical and Electrical Engineering, China University of Mining and Technology, Xuzhou 221116, China

Jiande Li
National Center of Quality Supervision and Inspection on Deep Processing Silicon Products, Lianyungang 222300, China

A simple method for fabricating line patterns on a superhydrophobic surface is demonstrated using nanosecond laser direct writing. A laser-induced superhydrophobic surfaces exhibit the excellent superhydrophobicity with a contact angle of 158° and a sliding angle of less than 5°. By changing the superhydrophilic linewidth and line intervals, the authors investigated the anisotropic wetting and adhesive properties on the as-prepared line-patterned superhydrophobic surface. The experimental results showed that the linewidth and line intervals have an important influence in anisotropic wetting, including contact angles and sliding angles in both parallel and perpendicular directions. This data allow control of adhesion by having droplets slide off at designated tilting angles on the patterned superhydrophobic surface. The water droplet array can be easily separated into any configuration, such as an upper triangular array. The as-prepared patterned superhydrophobic surface can transfer different microliter-sized droplets from one superhydrophobic surface to another. This patterned superhydrophobic surface has some potential applications for the droplet manipulation, microfluidic devices, and cell culture. © 2016 American Vacuum Society.
[http://dx.doi.org/10.1116/1.4966617]

I. INTRODUCTION

In recent decades, surfaces with special wettability have been sought after for both scientific and industrial applications. Inspired by lotus flowers,[1–4] scientists have designed a number of low-adhesive superhydrophobic surfaces with high contact angle (greater than 150°) and ultralow sliding angles less than 10° for use in self-cleaning,[5,6] anti-icing,[7] and drag-reduction[8] applications. Some highly adhesive superhydrophobic surfaces based on rose petals have also been recently reported. Superhydrophobic surfaces with high adhesion can maintain a contact angle of greater than 150°. Meanwhile, the droplet is pinned at the surface, even with the surface vertical or upside down.[9] Such a high-adhesion superhydrophobic surface has many potential applications in no-loss microdroplet transportation.[10]

Anisotropic superhydrophobic surfaces inspired by rice leaf have different sliding angles in different directions. These surfaces are attracting significant attention for their unique property of driving liquid along a preset path, which could potentially be applied in microfluidic devices, directional water-collection, and lab-on-chip systems.[11–13] Wu

et al.[14] achieved three-level biomimetic rice-leaf anisotropic superhydrophobic surfaces containing micro/nanostructures and macrogrooves produced by photolithography. Yang[15] reported 3D holographical nanostructured surfaces. These surfaces revealed anisotropic wettability and superhydrophobicity after SF_6 plasma treatment. Yong[16] used a femtosecond laser to produce an anisotropic polydimethylsiloxane surface, and achieved anisotropic wettability by adjusting the distance between two laser-induced superhydrophobic lines.

A superhydrophilic surface with a contact angle of nearly 0° is another extreme wetting surface, which can be widely used in antifogging, antifouling, and self-cleaning.[17] Recently, surfaces with both superhydrophilic and superhydrophobic properties have attracted considerable interest by many scholars. These special superhydrophilic–superhydrophobic patterns were first noted on the creatures, such as the Namib Desert beetle,[18] salviniamolesta,[19] and cups of lichens.[20] Inspired by these creatures, many superhydrophilic–superhydrophobic patterns have been fabricated using various technologies,[21,22] including the photomask-induced method[23] and the inkjet-induced method.[24] Tadanaga et al.[25] reported the fabrication of superhydrophilic–superhydrophobic TiO_2/Al_2O_3 patterns' surface on the surface of soda lime

[a]Electronic mail: Liuht100@126.com

glass. The flowerlike Al_2O_3 film was first coated on soda lime glass plates through a dipping–withdrawing approach. Then, a thin TiO_2 film was coated on the Al_2O_3 film. After fluoroalkyl silane modification and UV irradiation under a photomask, the superhydrophilic–superhydrophobic TiO_2-Al_2O_3-patterned surface was demonstrated. Zhang *et al.*[26] fabricated TiO_2-SiO_2 superhydrophilic–superhydrophobic patterns using a combination of spin-coating and photolithography. The resulting chips exhibited good stability and potential as function-integrated microchips. Fujishima *et al.*[24] proposed a new method for fabricating TiO_2-AL_2O_3superhydrophilic–superhydrophobic patterns on an Al plate without the use of a photomask using an inkjet-induced method. Lyu *et al.*[27] used a facile stamp method to fabricate superhydrophilic–superhydrophobic surface on a Cu substrate. Wang *et al.*[28] fabricated a superhydrophilic–superhydrophobic carbon nanotube/polybenzoxazine coating using a blade cutting. Kang *et al.*[29] proposed a mussel-inspired one-step surface modification method on a polymer coating to fabricate hydrophilic–superhydrophobic patterned surfaces. Some of the discussed synthesis strategies for superhydrophilic–superhydrophobic surfaces usually utilized the UV sensitivity of TiO_2, which allows TiO_2 film to switch its wettability property from superhydrophobicity to superhydrophilicity following UV irradiation. Some of the preparation methods use soft-lithographic techniques. These involve contacting the patterned mold with the superhydrophobic or superhydrophilic surface to prevent the hydrophobic or hydrophilic solution from contacting the entire superhydrophobic or superhydrophilic surface. Recently, some methods that do not use a photomask have been reported, like electrolyte jet machining techniques,[30] micromilling,[31] and femtosecond laser machining.[32] However, nanosecond laser direct writing technology is a novel technology for preparing superhydrophilic patterns on superhydrophobic surfaces. A nanosecond laser is a compact device that is cost effective and high efficient for manufacturing. It can fabricate different kinds of patterns such as squares, triangles, or circles on different metal superhydrophobic surfaces. The limited

research on this laser has investigated the change of anisotropic wettability for a single superhydrophilic line, but the influence of line interval on the anisotropic wettability has not been reported in detail.

Here, a fast and simple method is used to obtain line patterns on a superhydrophobic surface, with demonstrated anisotropic wetting and controllable adhesion. We first fabricated a rough surface using nanosecond laser-direct writing technology and modified fluoroalkyl silane to achieve superhydrophobicity. A superhydrophilic line pattern was achieved using the laser direct writing system. The as-prepared patterned lines on the superhydrophobic surfaces exhibited different anisotropic contact angles ($\Delta\theta$) and sliding angles in orthogonal directions for various linewidths and line intervals. Moreover, adhesion for different volume of the water droplets could be modulated by changing of linewidth and line intervals. This is applicable for transporting different sizes of water droplets to both high- and low-adhesive superhydrophobic surfaces.

II. EXPERIMENTAL METHODS

A. Materials

A 316L-type piece of stainless steel was selected as a substrate. The sample was mechanically polished, then cleaned for 30 min in an ultrasonic bath of *n*-hexane, rinsed with deionized water and acetone, and dried in a dry box. FAS-17 (1H, 1H, 2H, 2H-perfluorodecyltriisopropoxysilane) (97%) was purchased from SICONG chemical.

B. Fabrication of superhydrophobic–superhydrophilic line-patterned surface

Figure 1 shows a schematic diagram of the process of patterning a superhydrophilic line on the superhydrophobic surface. First according to our reported work,[33] the dried surface was mounted perpendicularly on the sample platform and then irradiated by a focused laser beam through a homemade laser marker with a focus lens (f = 160 mm) that can control the motion of the focused laser beam in the x–y
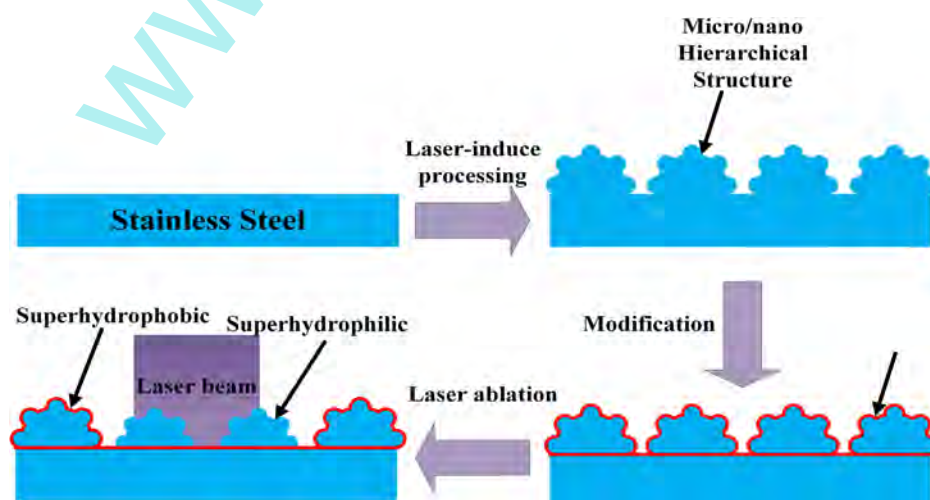

FIG. 1. (Color online) Schematic diagram of process for fabricating superhydrophobic–superhydrophilic line-patterned surface.

direction. A 25-ns ultraviolet laser with a working wavelength of 355 nm and repetition rate of 6.8 kHz was selected as a laser source. In the laser-induced superhydrophobic surface step, the laser power was fixed at 31.5 J/cm^2, the laser scanning space was 20 μm, and the laser scanning velocity was 5.28 mm/s. Following the irradiation process, samples were cleaned with distilled water and dried at 60 °C for 1 h. Then, dried, laser-processed samples were immersed into a 2 wt. % FAS-17 (1H, 1H, 2H, 2H-perfluorodecyltriisopropoxysilane) ethanol solution for 1 h followed by washing with ethanol and drying in an oven at 100 °C for 1 h. After surface modification, the laser-induced surface exhibited excellent superhydrophobicity. For line patterning step, the as-prepared superhydrophobic surface was mounted perpendicularly on the sample platform and irradiated by a focused laser beam again. The laser fluence was varied from 6.26 to 31.50 J/cm^2, and the laser scanning space varied from 600 to 1200 μm at a fixed scanning velocity of 5.28 mm/s. Finally, samples were rinsed with *n*-hexane and acetone in an ultrasonic bath and dried in a dry box at 80 °C for 30 min.

C. Characterization

Surface morphologies of all the samples were observed using a scanning electron microscope (FEI limited, Quanta 250). The sample compositions were characterized by x-ray photoelectron spectroscopy (XPS). The water contact angle and sliding angle of 2–20 μl deionized water droplets were measured using the JC2000D-2A contact angle measuring device on five different points for each surface. The micro-roughness sample surface was characterized using a Bruker's Dektak XT stylus profilers. The AFM (CSPM5500 electronics, Benyuan Nano-Instrument, China) was used to measure the nanoroughness of the as-prepared surface. A high-speed digital microscopic system (VW-9000, KEYENCE) was used to capture the air–solid–liquid three-phase contact area.

III. RESULTS AND DISCUSSION

A. Surface morphology and wetting behavior of patterned superhydrophobic surface

Figure 2(a) shows a SEM image of the as-prepared super-hydrophobic stainless steel surface consisting of highly uniform self-assembled microprotrusions and microcavities. The high magnification SEM image in Fig. 2(b) shows that each microprotrusion was decorated by tens or hundreds of nanostructures, which reveals a large area of hierarchical micro/nanostructures. Figures 2(c) and 2(d) show that the water contact angle and sliding angle of the as-prepared superhydrophobic surface were 158° and 5°, respectively, for a 5 μl water droplet. The water droplet was spherical in shape and easily rolled off when the entire rough surface was tilted 5°. Figure S1 shows the profile curves of the as-prepared superhydrophobic surface and a polished surface.[54] The size and height of microprotrusions were approximately 16 ± 5 and 8 ± 2 μm, respectively. The depth of microcavities was about 4.5 ± 2 μm. The surface roughness (Ra) is ~3.34 μm. The inset of Fig. 2(b) shows the AFM image of
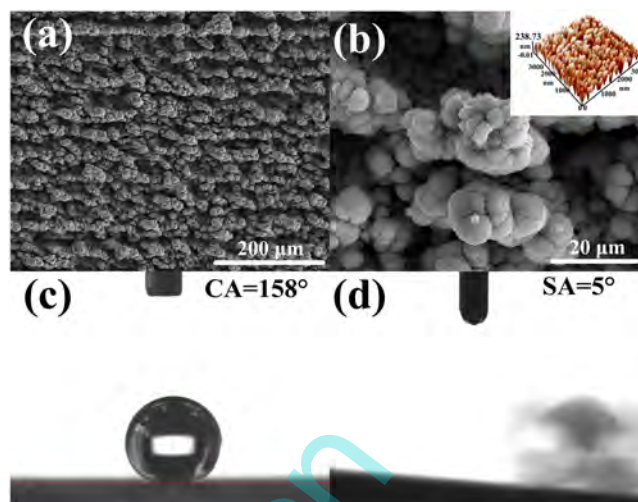

FIG. 2. (Color online) SEM images of superhydrophobic surface and its contact angle and sliding angle. (a) The SEM image of superhydrophobic surface at 500× magnification. (b) The SEM image of superhydrophobic surface at 4000× magnification. (c) Image of the contact angle on the as-prepared superhydrophobic surface. (d) Image of sliding angle on the as-prepared superhydrophobic surface.

our prepared surface. The roughness was ~59.7 nm. The as-prepared superhydrophobic surface clearly shows the roughness on the nanoscale as well as microscale. Thus, this hierarchical micro/nanoroughness surface is rough enough to achieve excellent superhydrophobicity. This excellent super-hydrophobicity can be well explained using the Cassie model,[34] in which air trapped within the hierarchical micro/nanostructures beneath the liquid forms a composite solid–liquid–vapor interface.[35]

In order to investigate the formation mechanism of hierarchical micro/nanostructures induced by nanosecond laser ablation, we compared SEM images of the dynamic formation process of hierarchical micro/nanostructures with low laser fluence and high laser fluence shown in Figs. S1 and S2. For the structures with low laser fluence, after the first line of laser scanning, an ablation line appeared on the stainless steel surface. The internal surface of this line was relatively smooth. Some particles and cracks were randomly distributed at the edge of remelting structure, as shown in Fig. S2(a). As the scanning line number (Ns) increases to 3, uniformly distributed microbumps were formed at the location of the previous scanning line, as shown in Fig. S2(c). This results in gradual formation of recast layer caused by the overlap between lines. The recast layer would be pushed forward and accumulates in the moving direction and finally forms microbumps. Generally, when the laser pulse fluence is low, the melting area first occurs on the material surface. Then, evaporation occurs from the melting surface. Thus, the main removal forms are melting and evaporation. The depth of the removed material in the ablated area is tens of nanometers. The ablated area should to be smooth, and, thus the appearance of the microbump is smooth. When Ns = 50, the recast layer accumulates enough remelting structure to form uniform distributed microbumps. For the structures with high laser fluence, after the first laser scanning line, as

shown in Fig. S3(a), more roughness is visible on the internal surface compared to those with low laser fluence. This can be mainly attributed to the fact that when the fluence of a focused laser beam is higher than the "strong" ablation[36] ($\Phi_{strong} = 2.5$ J/cm^2), the ablated surface absorbs a large amount of heat, which forms a localized melting pool.[37] Then, when the surface temperature increases to some breakpoint, a large amount of vaporization nuclei appear in the melting layer. The melting layer changes to microdroplets, which burst out of the focal spot when the steam pressure on the melting material is greater than the surface tension of the melting liquid. Meanwhile, the recoil pressure on the melted surface results in the formation of a microcavity.[38] Moreover, electrons around the irradiated region break down into dielectrics, rapidly ionize, and eventually form plasma[39] due to some nonlinear effects such as multiphoton and avalanche ionization.[40] The plasma will interfere with energy absorption of the ablated surface and cause splashing droplets to be redeposited in the ablated region.[41] Here, tens or hundreds of self-assembled nanoprotrusions appeared at the edge of the microstructure for the redeposited ejected particles. The length of the recast layer increases as N continuously increases in the moving direction, as shown in Figs. S3(c)–S3(e). Thus, a large area of hierarchical micro/nanostructures is fabricated by nanosecond laser irradiation on stainless steel when the scanning line number was large enough.

After laser scan line patterning on the superhydrophobic surface, the original superhydrophobic structures were found to be destroyed by the intensive laser-generated heat. Figure 3 shows the SEM images of the superhydrophilic line at different laser powers. It can be clearly seen that a new laser ablated line was present on the superhydrophobic surface. The internal surface of the new line contains smooth microbumps and micropores. The variations in linewidth as a function of laser power can be easily measured using the scale bar of SEM image, as shown in Fig. 3(d). The width of the newly generated line increased with increasing laser power. This is because the distribution of laser fluence is in concordance with Gaussian distribution. A higher laser power means a larger ablated diameter, which can achieve a wider scanning line. Thus, we can control the width of a scanning line by changing the laser fluence. The transformation from superhydrophobicity to superhydrophilicity is mainly due to the changes in chemical composition caused by laser ablation on the superhydrophobic surface and the capillary effect on the newly generated microprotuberance. Figure 4(a) shows a XPS high-resolution spectrum of F1s on the superhydrophobic area. The F1s peaks located at 687.14 and 688.05 eV correspond to the carbon atoms of $-CF_3$ and $-CF_2-$, respectively. Figure 5(b) shows a XPS high-resolution spectrum of F1s on the secondary laser ablated area on the superhydrophobic surface. There is no obvious spectral peak of F1s, which means that FAS-17 molecules must disappear after laser ablation on the superhydrophobic surface. The main reason for this phenomenon is the thermal decomposition of FAS-17 molecules. When the temperature is higher than 250 °C, the CF_2 and CF_3 groups begin to decompose, and at 450 °C, they are almost completely decomposed.[42] It is clear that the temperature of the laser focus spot that can melt stainless steel (melting point about 1440 °C) is much higher than the complete decomposition
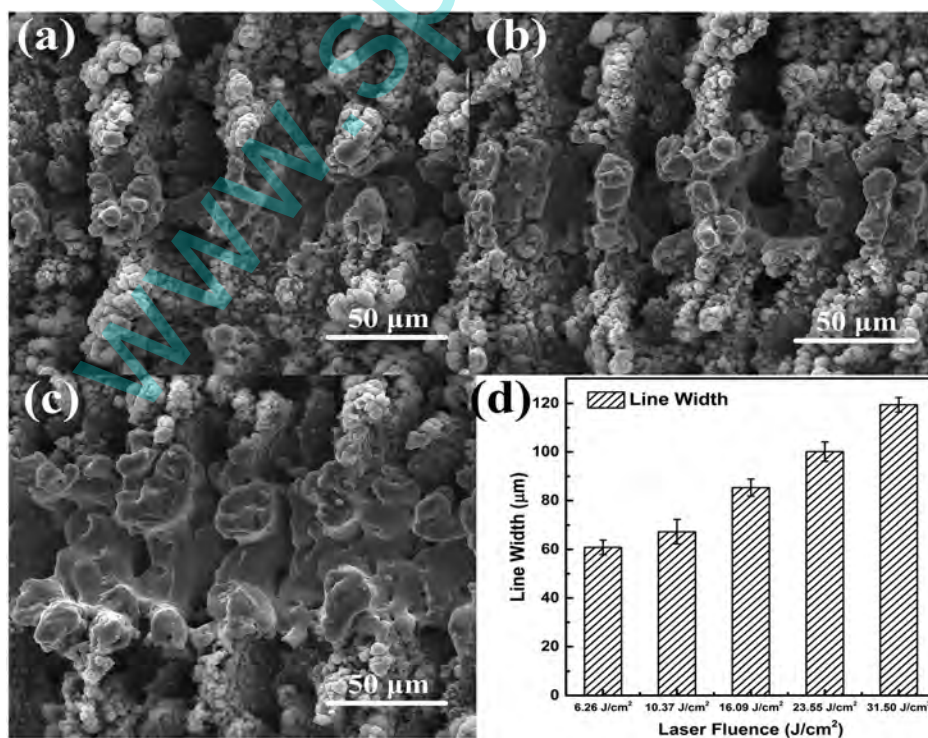

FIG. 3. SEM images showing morphologies of superhydrophilic lines with different laser powers: (a) 6.26 J/cm^2, (b) 10.37 J/cm^2, (c) 31.5 J/cm^2, and (d) a histogram of line width for different laser fluences.
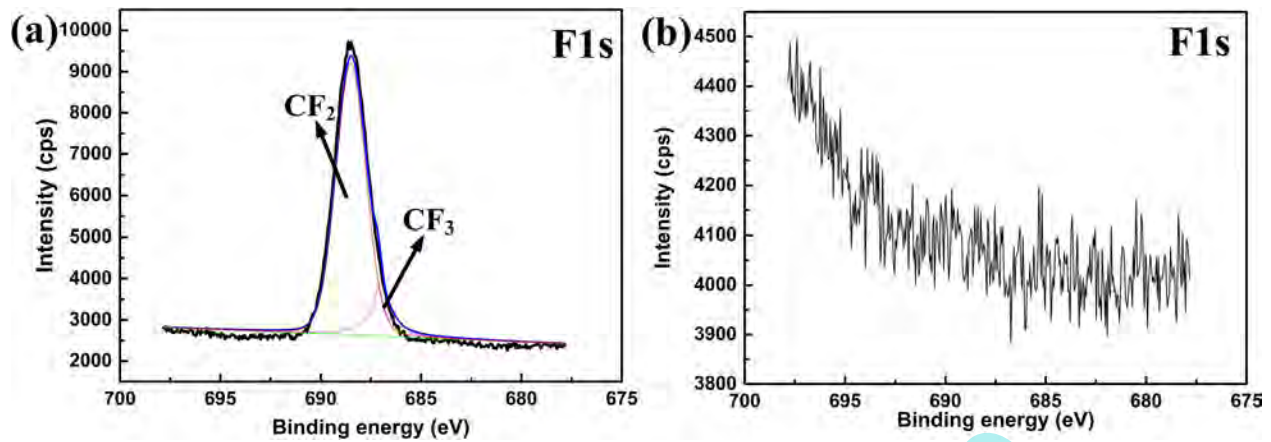
FIG. 4. (Color online) XPS high-resolution F1s spectrum of (a) the superhydrophobic surface and (b) the secondary laser-ablated area on the superhydrophobic surface.

temperature for the FAS-17 molecule. Figure 5(a) shows the top view of the air–solid–liquid three-phase images by microscope and a side view when the sample was completely immersed in water. From the dark/bright contrast in Fig. 5(b), the dark zone follows the superhydrophilic line track, which means that water fully wet microstructures obtained by secondary laser scanning. This is highly consistent with the Wenzel model.[43] Thus, water can adhere very well on the superhydrophilic line. The bright zone is indicative of the reflection of light from the trapped air layers between the superhydrophobic surfaces away from the superhydrophilic line and the water. Figure 5(b) displays the top view of the air–solid–liquid three-phase images by microscope and its side view when the sample was taken out from the water. It

clearly can be seen that the bright water is stuck on the scanning line and the dark zone still retains superhydrophobicity. This demonstrates that our as-prepared superhydrophobic surface agrees well with the Cassie model owing to the discontinuous three-phase contact line (TCL) and a large volume of air trapped between the liquid and microstructures.[44]

B. Anisotropic wetting

On the basis of these results, we further investigated the anisotropic wetting behavior of the superhydrophilic line pattern on the superhydrophobic surface with different laser fluences and line intervals. We measured both the static contact angles and sliding angles to determine the anisotropic
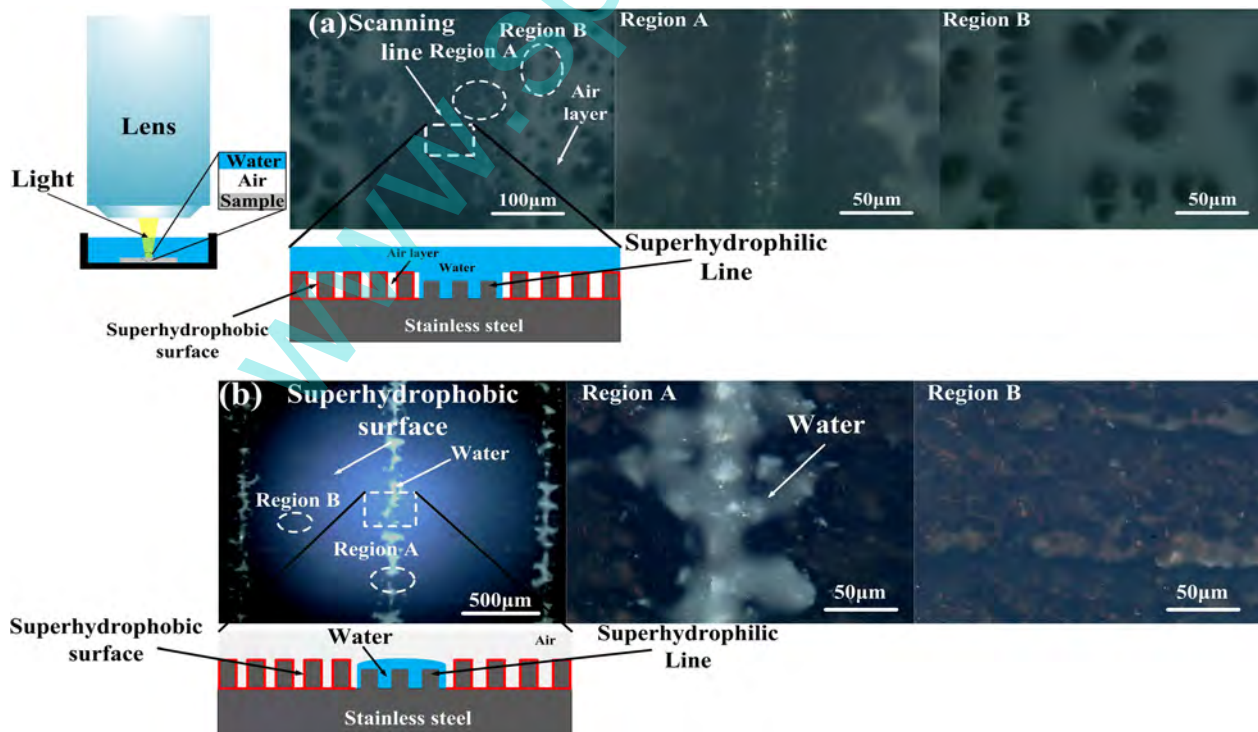

FIG. 5. (Color online) Microscope images of liquid–solid–vapor interface of line-patterned superhydrophobic surface. (a) The sample was completely immersed into water, and (b) the sample was taken out from the water.

wettability of the superhydrophilic line pattern on the super-hydrophobic surface. Here, we measured the contact angles in the parallel and perpendicular directions to the line-patterned superhydrophilic–superhydrophobic surface as $\theta c_{\parallel}$ and $\theta c_{\perp}$ with a droplet volume of 8 μl. Figure 6(a) shows the relationship between contact angles in the parallel and perpendicular directions and laser fluence with of 8 μl droplet volume on the single line. In the perpendicular direction, the contact angles decreased slightly with increasing of laser fluence. In the parallel direction, the contact angles decreased greatly with increasing laser fluence. Next, the $\Delta\theta = \theta_{c\perp} - \theta_{c\parallel}$ was calculated to evaluate the anisotropic wetta-bility in two directions. As shown in Fig. 6(b), $\Delta\theta$ increased with increasing laser fluence. This anisotropic wetting phe-nomenon can be explained by the following reasons. First, the water would adhere the superhydrophilic line due to the capillary effect[45] and thermal decomposition of FAS-17 molecules, resulting in the water enhancing the directional spreading of the water droplet in the parallel direction. The air bubble can be clearly seen between the surface and water droplet, which may push out from microstructures in the line generated by high laser fluence, as shown in the inset of Fig. 6(a). The droplet was elongated along the superhydrophilic line. Then, on the untreated surface, the water droplet can easily roll off at a small tilt angle, resulting in an unsteady state. On the other hand, the water droplet can be completely absorbed by the superhydrophilic line, leading to a stable state. According to Gibbs' criterion, the unsteady state means that the object is in a higher energy and the stable state has a lower energy. Thus, the water droplet needs to overcome an energy barrier forming between the highest energy superhydrophobic surface and relatively lower energy superhydrophilic line.[46,47] When the water droplet first touches the superhydrophilic line, the line's high adhe-sive force induces the droplet to spread in the parallel direc-tion. Meanwhile, the superhydrophobic surface with high energy prevents the water from moving in the perpendicular direction. As a result, the contact angle in the perpendicular direction is higher than that in the parallel direction. The linewidths increased with increasing laser fluence. Thus, the

interfacial widths increased with the increasing linewidths, showing that droplets have the trend to cover wide linewidths.

Figure 7(a) shows contact angles with different grating periods with respect to droplet volume and tilting direction when the laser fluence is 31.5 J/cm². In the perpendicular direction, the contact angles exhibited different trends with increasing line interval and droplet volume. When the line interval was ~500 μm, the contact angles changed sharply change points at droplet volumes of 4 and 10 μl. The contact angles also changed suddenly at a droplet volume of 6 μl when the line interval increased to 1000 μm, again at a drop-let volume of 10 μl when the line interval was 1500 μm. Then, the $\Delta\theta = \theta_{c\perp} - \theta_{c\parallel}$ was calculated, as shown in Fig. 7(b). The changing trends of $\Delta\theta$ with different line intervals were consistent with those observed for contact angles in the perpendicular direction. These sudden changes in the contact angle or $\Delta\theta$ can be attributed to the fact that a droplet can contact different superhydrophilic line numbers as the drop-let volume increases. Figure 8(a) presents a series of sche-matic diagrams expressing the sudden change in the contact angle when the water is dropped on an as-prepared surface with a 500-μm line interval. As the water volume increases, the water contacts more than one superhydrophilic line. The contact angle would then suddenly decrease when the water contacts two or three superhydrophilic lines. According to the geometric relationships between the contact angle and drop radius (R) on the superhydrophobic surface, as shown in Fig. 8(b), we can calculate the theoretical contact diame-ters of the superhydrophobic surface at different water vol-umes according to

$$D_a = 2 \times \sqrt[3]{\frac{3V}{4\pi}} \sin\theta, \tag{1}$$

where D_a is the theoretical contact diameter, V is the water volume, and θ is the experimental contact angle. According to the known linewidth and line intervals shown in Fig. 10(c), we can calculate the real contact length of the super-hydrophobic area according to
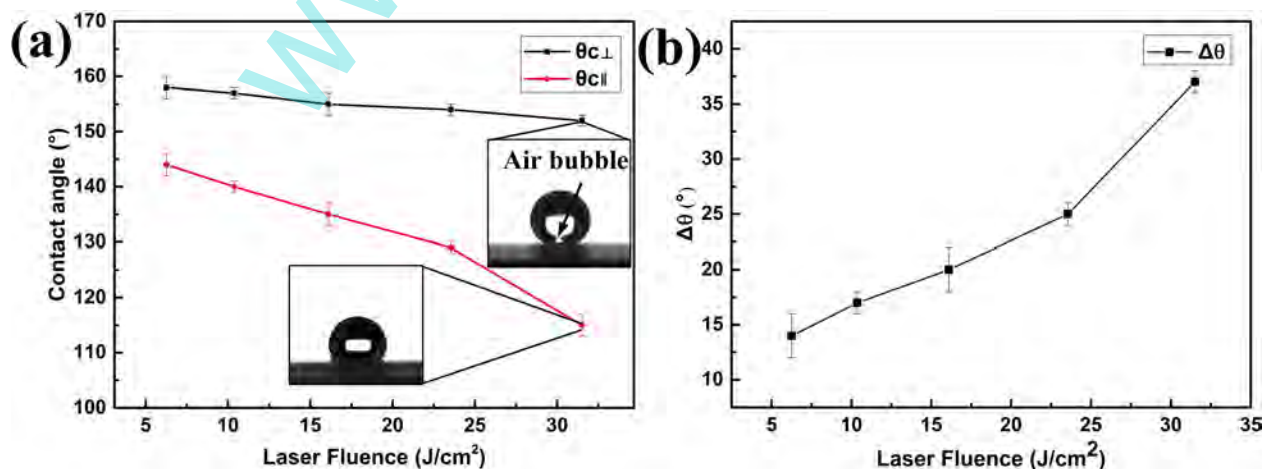

FIG. 6. (Color online) Plot of the contact angles (a) and $\Delta\theta$ (b) of 8-μl droplet on the single-line superhydrophobic surface fabricated at different laser fluences.
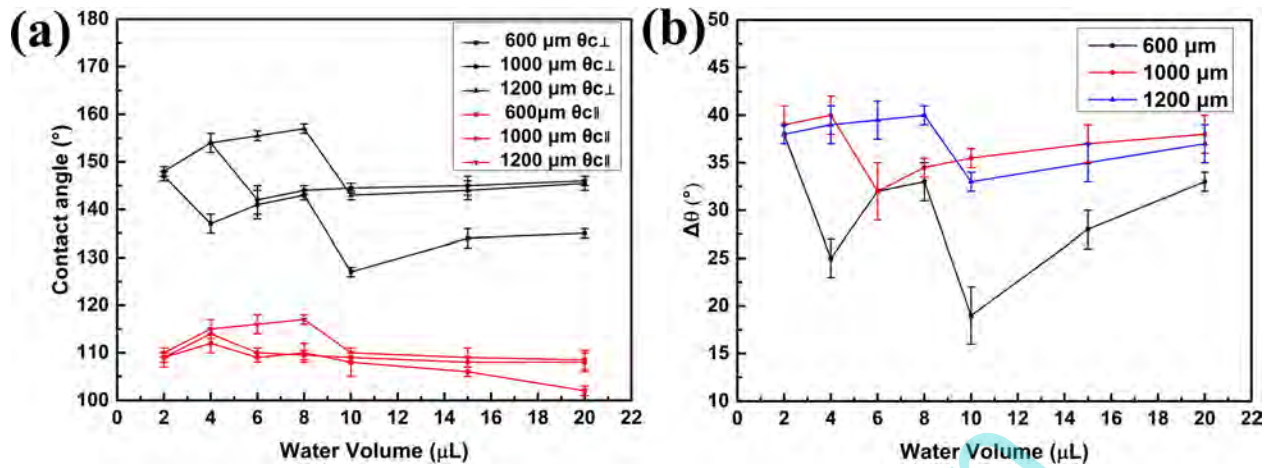
FIG. 7. (Color online) (a) Parallel and perpendicular contact angles and (b) $\Delta\theta$ of droplets with different volumes on a patterned superhydrophobic surface with different line intervals.

$$D_i = |(N - 1) \times D_s - D_w|, \quad (2)$$

where D_i is the real contact length of the superhydrophobic area, subscripts i and N indicate the number of the superhydrophilic line that contacts the water droplet, D_s is the line interval, and D_w is the linewidth. Thus, we can obtain the theoretical line number (N_t) of water contact after the comparing of the theoretical contact diameter (D_a) for different

water volumes and the real contact length of superhydrophobic area (D_i), according to

$$N_t = \begin{cases} 1, & D_a \leq D_2 \\ 2, & D_2 \leq D_a \leq D_3 \\ 3, & D_3 \leq D_a \leq D_4. \end{cases} \quad (3)$$

As shown in Fig. S4, the theoretical contact diameter increases with increasing droplet volume. Different theoretical water-contacting line numbers (N_t) can be obtained for the different line intervals (D_s) ($D_s = 600$, 1000, and 1200 μm). As shown in Fig. S4(a), when the line interval D_s is ~600 μm, the water droplet contact would be just pinned by a single superhydrophilic line at the 2 μl volume and then contact two superhydrophilic lines when the water volume increased to 4 μl. The water droplet would contact three superhydrophilic lines when the water volume increased to 10 μl. Thus, the contact angles change suddenly at the 4 and 10 μl volume adhering to the superhydrophobic surface with a 600-μm line interval. This result is highly consistent with the sudden changes in the contact angle or $\Delta\theta$ in Fig. 7. Thus, we can utilize this anisotropic wettability strategy to control the motion of a water droplet in a predetermined path.

C. Anisotropic sliding property and controllable adhesion force

The laser-ablated line on the superhydrophobic surfaces exhibited directionally controlled droplet sliding angles. Figure 9(a) shows the sliding angles in the parallel ($SA_{//}$) and perpendicular directions ($SA_{\perp}$) on the single line with different laser fluences for a constant droplet volume of 10 μl. The $SA_{//}$ varied slightly with increasing laser fluence, while $SA_{\perp}$ increased greatly. Thus, the anisotropic sliding property becomes predictable with increasing laser fluence. The anisotropic sliding property can be mainly explained by the motion of the TCL toward the sliding direction[48,49] and the energy barrier between the superhydrophobic surface and superhydrophilic line. In general, the length and continuity of the TCL on the surface can influence the sliding
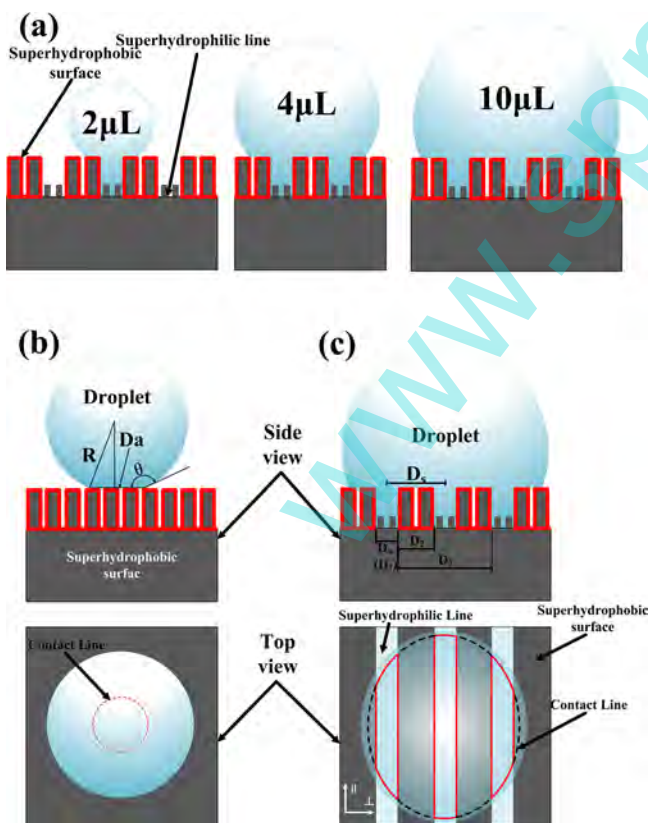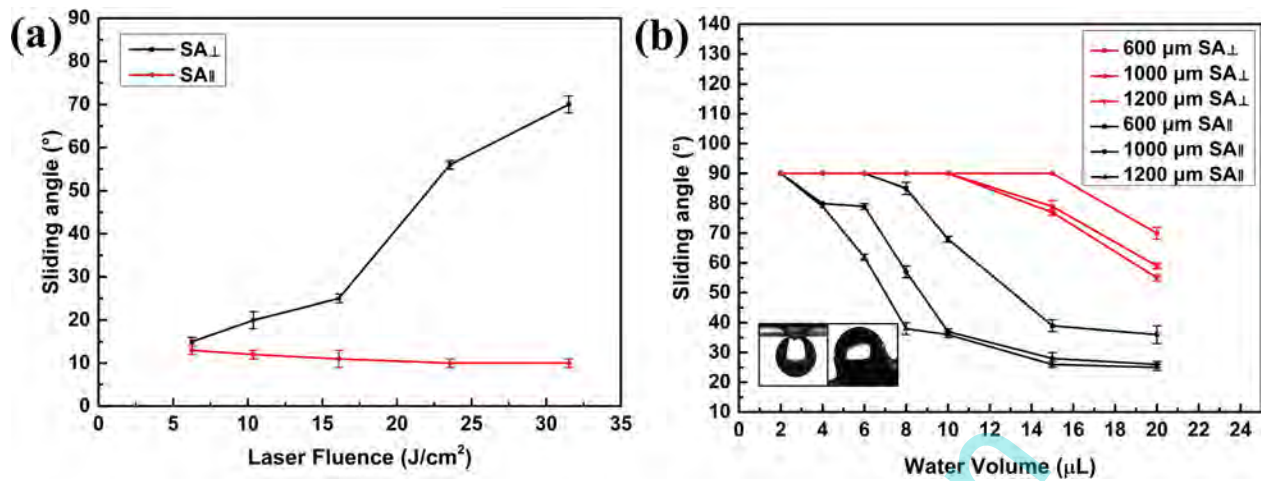

FIG. 8. (Color online) (a) Schematic diagrams of the change in contact angle when the water is dropped on sample 1. (b) The side view and top view of droplet on the superhydrophobic surface. (c) The side view and top view of droplet on the line-patterned superhydrophobic surface.

FIG. 9. (Color online) (a) Sliding angles of 10-μl droplet on the single-line superhydrophobic surface that were fabricated at different laser fluences. (b) Parallel and perpendicular sliding angles of droplets with different volumes on a patterned superhydrophobic surface with different line intervals.

property of the water droplet. A continuous, short TCL yields a better sliding behavior than a discontinuous and long TCL. The superhydrophilic lines can influence the profile, length, and continuity of a TCL. On the superhydrophilic line, the water droplet would wet, spread on the superhydrophilic line, and finally form a continuous TCL. On the superhydrophobic surface, the TCL is discontinuous and homogeneous distribution and thus can lead to isotropic wettability. Thus, on the line-patterned superhydrophilic–superhydrophobic surface, the water droplet would form both discontinuous and continuous TCLs, which can change the shape of TCLs as well as the shape of droplets.[50] Furthermore, an energy barrier can form between adjacent superhydrophobic surface and superhydrophilic line. As a result, when the droplet is sliding in the parallel direction, there is no energy barrier on the superhydrophilic line. However, when the droplet is sliding in the perpendicular direction, the water would first overcome the energy barrier from a low-energy superhydrophilic line to a high-energy superhydrophobic zone and then slide away from the surface.

Figure 10 shows the schematic illustration of the anisotropic sliding mechanism on a line-patterned superhydrophobic surface. In the parallel direction, the droplets need to overcome the viscous force F_{vis} of water in the superhydrophilic regions and the negligible adhesive force F_{ads} between droplets and the superhydrophobic areas. In the perpendicular direction, the droplet would mainly need to overcome the adhesive force F_{adsh} between droplets and superhydrophilic areas and adhesive force F_{ads} between droplets and the superhydrophobic areas. F_{adsh} is much larger than F_{vis} due to the fact that the viscous force F_{vis} can be ignored at very low sliding velocities. Because of the difference in force between the two directions, droplets sliding along parallel direction slide much more easily than in the perpendicular direction, showing obvious anisotropic sliding property. In order to further explain the influence of line width and line intervals on the sliding angle, we calculated the overall adhesive force according to Eq. (4)

$$F_{ad} = F_{adsh} + F_{ads} = A_{\text{Line}}\gamma_{LV}(\theta_{LR} - \theta_{AD}) + (A_{\text{droplet}} - A_{\text{Line}})\gamma_{LV}(\theta_R - \theta_{AD}), \quad (4)$$

where A_{Line} is the droplet line interfacial area, θ_{LR} is the receding contact angle of the superhydrophilic region, and θ_R and θ_{AD} are the receding and advancing contact angles on

FIG. 10. (Color online) Schematic illustration of a droplet sliding off the line pattern in directions: (a) top view, (b) parallel to the line, and (c) perpendicular to the line.

the laser-induced superhydrophobic surface, respectively. $A_{droplet}$ is the overall droplet–substrate contact area. Here, the droplet groove interfacial area is related to the linewidth and the droplet-contacting line number. When the droplet volumes were kept constant, the interfacial areas increased with increasing linewidths, indicating that droplets have the tendency to spread on lines with greater widths, which means higher adhesive force. It has been demonstrated that the linewidth increases with laser fluence. Hence, the $SA_{\perp}$-values were greatly affected by the laser fluence, while $SA_{//}$-values slightly decreased with laser fluence.

Figure 9(b) shows sliding angles in the parallel and perpendicular directions for various droplet volumes and line intervals at a laser fluence of 31.5 J/cm^2. The sliding angles in both parallel and perpendicular directions decreased with increasing water droplet volume because gravity was greater than the adhesion force on the high adhesive line. All the samples exhibited different degrees of anisotropic sliding properties for different water droplet volumes and line intervals. Moreover, the line-patterned superhydrophobic surfaces with 600-μm line intervals had larger sliding angles than the surface with 1200-μm line intervals. This is mainly due to the fact that the water droplet would contact different number of superhydrophilic lines at the constant droplet volume for the superhydrophobic surface with different line intervals. According to the Eq. (3), $SA_{\perp}$ is determined by the

adhesion force F_{adsh}. A_{Line} is the key element for the adhesion force F_{adsh}. For a constant droplet volume, the smaller line intervals can lead the droplet to contact more superhydrophilic lines, corresponding to a larger droplet line interfacial area. The larger A_{Line} means higher adhesive force. For constant line intervals, the droplet line interfacial area increased with increasing droplet volumes. Thus, we can control the sliding angle and adhesive force of as-prepared line-patterned superhydrophobic surfaces by adjusting the laser fluence and laser scanning intervals.

D. Applications

In Sec. III C, it was shown that the patterned superhydrophobic surface has a strong anisotropic wettability. The underlying mechanism is that the line pattern created by laser ablation locally increased solid–liquid adhesion.[51,52] We therefore explore the potential applications of patterned superhydrophobic surfaces on some typical microdroplet manipulation processes. Compared with the random location and easy slide-off on uniform superhydrophobic substrates, the patterned superhydrophobic substrates have good adhesion and fixed location to attract liquid droplets. These unique properties make the patterned superhydrophobic surface a favorable substrate for storing and separating droplets of expensive test fluids and reagents in a stable and visible manner. As shown in Fig. 11(a), a 5×5 arrayed single line
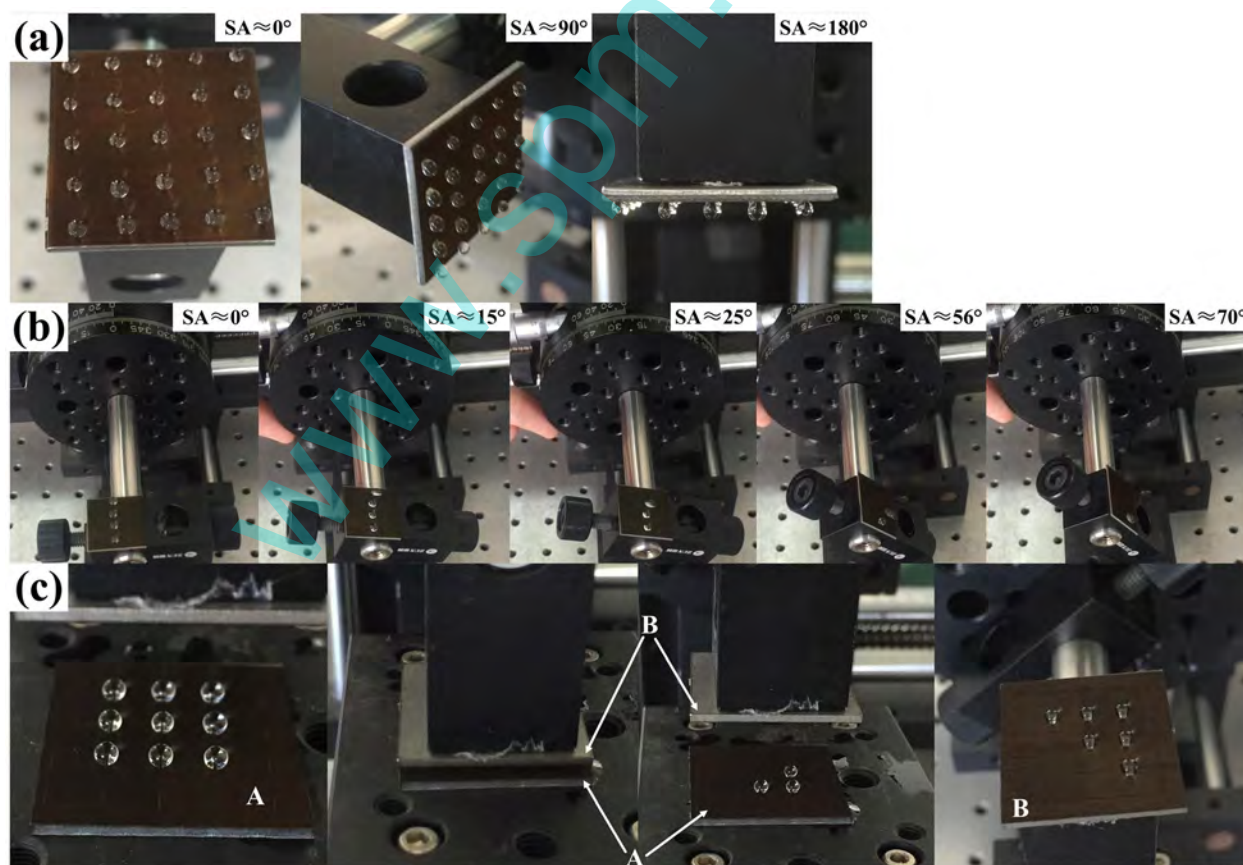

FIG. 11. (Color online) Applications of line patterns on superhydrophobic surface: (a) Water droplets of 8 μl stuck firmly on the 6×6 single-line arrays, which were processed by laser fluence of 31.5 J/cm^2 with laser scanning velocity of 5.28 mm/s. (b) Droplets slide off at different angles by using different laser fluences. (c) The dynamic process of a 3×3 water arrayed droplet separating into lower triangular-arrayed droplets and upper-triangular arrayed droplets.

pattern, processed by laser fluence of 31.5 J/cm^2 and laser scanning velocity of 5.28 mm/s, was obtained on the as-prepared superhydrophobic stainless steel surface. The spacing between each line was 5 mm. Water droplets with volumes of 8 μl remained steadily on the patterned surface and did not slide off even when the surface was rotated 90° or 180°. The laser fluence can be used to control the sliding angles of line-patterned superhydrophobic surfaces, thus allowing fabrication of lines with different laser powers at specified positions. The droplets could slide at designated angles with or without residual water left on a line. Figure 11(b) shows four 10-μl droplets on a line-patterned superhydrophobic surface (left to right). The four lines on the superhydrophobic surface were processed with a laser scanning velocity of 5.28 mm/s at laser fluences of 6.26, 16.09, 23.5, and 31.5 J/cm^2. Four droplets gradually slide off the line in the perpendicular direction at about 15°, 25°, 56°, and 70°, respectively. This demonstrated the ability to select a water droplet by designating a particular sliding angle. Due to the flexibility of laser processing, different kinds of line arrays can be fabricated on the superhydrophobic surface. This has an important potential application for droplet manipulation and separation. As shown in Fig. 11(c), the 3 × 3 arrayed droplets remained adhered to the as-prepared line-patterned superhydrophobic stainless steel surface (surface A). Then, an upper triangular-array line-patterned superhydrophobic surface (surface B) descends until it contacts and compresses the 3 × 3 arrayed water droplets. By lifting surface B up, the upper triangular-arrayed droplets are completely adhered to

surface B due to the higher water adhesive force. The lower triangular-arrayed droplets remain on surface A. Thus, droplets were successfully separated into lower triangular-arrayed droplets and upper triangular-arrayed droplets.

Utilizing anisotropic wettability, the motion of water droplet easily can be controlled by sliding along the predetermined path. Figure 12(a) shows a 20-μl droplet sliding along a predetermined curved line on the patterned superhydrophobic surface. With the help of gravitational force, droplets slide along the intended route when the sample tilts about 10°, where their direction to the final target area is guided by the adhesion anisotropy of the line (Movie S1 of the supplementary material). Two 10-μl water droplets located at two different lines of "Y-shaped" superhydrophobic surface would behave similarly. These two droplets would move to the lower position and mix with each other into a single 20 μl droplet at the end point of the Y-shape. Finally, the mixed droplet could slide off the sample by increasing the titling angle, as shown in Fig. 12(b). Not only can as-prepared patterned superhydrophobic surfaces be useful for droplet storage, mixing, and direction transfer, but also for spontaneous pumpless tilted transport. Figure 12(c) shows dynamic processes of a water droplet pumping up along an inclined superhydrophilic wedge-shaped track. Due to the unbalanced capillary forces in the lengthwise direction, the liquid along the wedge-shaped track is driven from a smaller wettable footprint (left) to a larger one (right).[53] It can be clearly seen that the capillary force produced on the droplet by the wedge-shaped track is also strong enough to
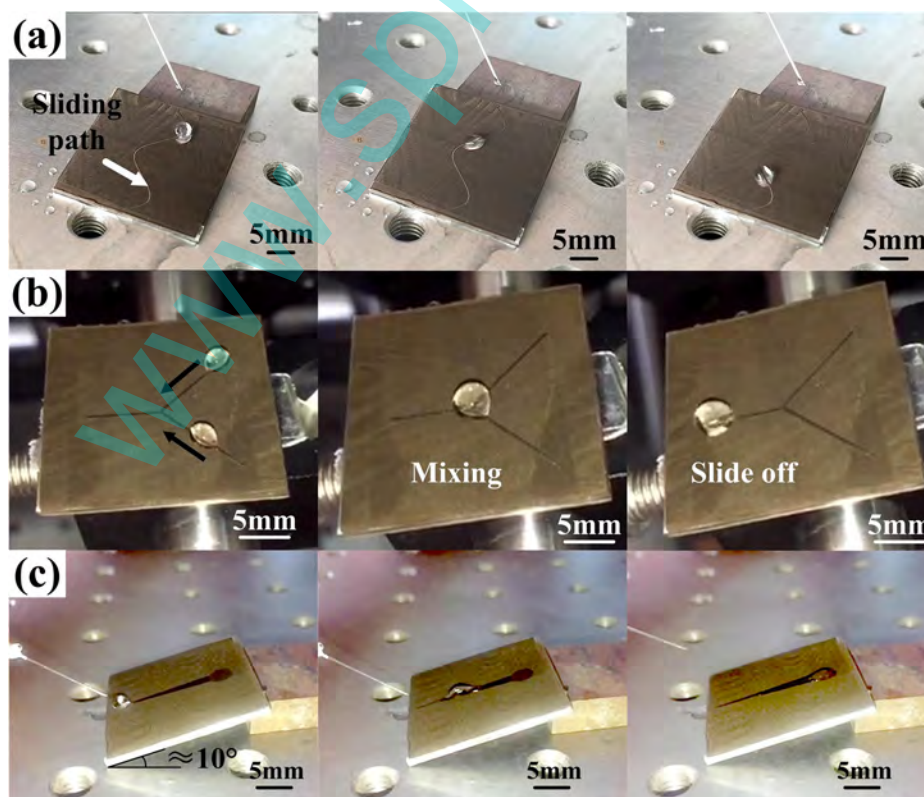

FIG. 12. (Color online) Dynamic manipulation of some typical microdroplets based on the patterned superhydrophobic surface: (a) droplet sliding along a curved line, (b) two droplets mixing, and (c) droplet spontaneous pumpless tilted transport.
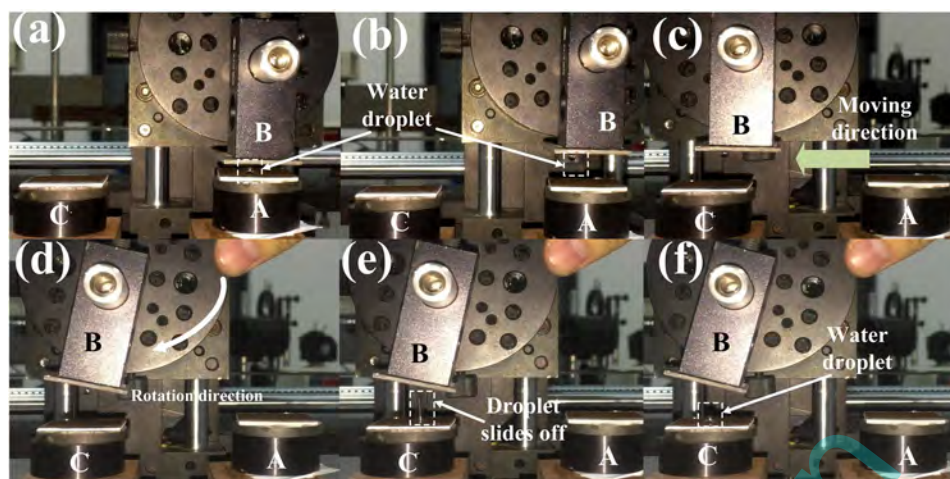
FIG. 13. (Color online) Snapshots of dynamic process of our prepared patterned superhydrophobic surface transferring a 15-μl water droplet from one superhydrophobic surface to another.

move the liquid up along an inclined substrate. The liquid is pumped up a ramp to an elevation of 4 mm (see the Movie S2 of the supplementary material). This corresponds to an approximate ramp tilt angle of 10° for the patterned superhydrophobic substrate.

In addition, owing to its anisotropic sliding ability and high adhesion property, we find that the as-prepared line-patterned superhydrophobic surface with line spacing of 600 μm also can be used as "mechanical hands" to transfer water droplets from one superhydrophobic surface to another. Figure 13 shows a series of snapshots of the dynamic process of our prepared patterned superhydrophobic surface transferring a 15-μl water droplet from one superhydrophobic surface (A) to another superhydrophobic surface (C) (see in the Movie, S3). First, the patterned superhydrophobic surface B (sample 6) adheres the water droplet on the superhydrophobic surface A, as shown in Figs. 13(a) and 13(b). Then, the surface B is placed over another superhydrophobic surface C, as shown in Fig. 13(c). Surface B is then tilted slightly. The water droplet slides along the superhydrophilic line and successfully falls onto another superhydrophobic surface C, as shown in Figs. 13(d)–13(f). This water droplet transfer ability has potential applications for drug delivery and lossless liquid transportation.

IV. CONCLUSIONS

Superhydrophobic surfaces were obtained by nanosecond laser processing. The as-prepared surfaces revealed excellent water repellence with a water contact angle of 158° and sliding angle of 3° after FAS-17 modification. Superhydrophilic lines were able to be fabricated on the as-prepared superhydrophobic surface due to the thermal decomposition of FAS-17 molecules. By adjusting the superhydrophilic linewidth and line intervals, we achieved control of anisotropic wettability and adhesion in orthogonal directions, suggesting the ability to transfer different microliter-sized droplets. Water droplets can be slide off at designated tilting angles of the patterned superhydrophobic surface. A water droplet array easily can be separated into any water droplet array, such as

an upper triangular-array. We demonstrate the dynamic process of capture or transfer microliter-sized droplets from the superhydrophobic surface to another superhydrophobic surface. Hence, this line-patterned superhydrophobic surface has potential applications for droplet manipulation, microfluidic devices, and cell culture.

ACKNOWLEDGMENTS

[1]A. Marmur, Langmuir **20**, 3517 (2004).
[2]S. Zheng, C. Li, Q. Fu, W. Hu, T. Xiang, Q. Wang, M. Du, X. Liu, and Z. Chen, Mater. Des. **93**, 261 (2016).
[3]X. Wu, Q. Fu, D. Kumar, J. W. C. Ho, P. Kanhere, H. Zhou, and Z. Chen, Mater. Des. **89**, 1302 (2016).
[4]I. Hejazi, G. M. M. Sadeghi, S. H. Jafari, H. A. Khonakdar, J. Seyfi, M. Holzschuh, and F. Simon, Mater. Des. **86**, 338 (2015).
[5]B. Zhang, X. Zhao, Y. Li, and B. Hou, RSC Adv. **6**, 35455 (2016).
[6]B. Zhang, Y. Li, and B. Hou, RSC Adv. **5**, 100000 (2015).
[7]M. Ruan, W. Li, B. Wang, B. Deng, F. Ma, and Z. Yu, Langmuir **29**, 8482 (2013).
[8]B. Bhushan and Y. C. Jung, Prog. Mater. Sci. **56**, 1 (2011).
[9]B. Bhushan and E. K. Her, Langmuir **26**, 8207 (2010).
[10]X. Hong, X. Gao, and L. Jiang, J. Am. Chem. Soc. **129**, 1478 (2007).
[11]B. Balu, A. D. Berry, D. W. Hess, and V. Breedveld, Lab Chip **9**, 3066 (2009).
[12]Z. Cheng, L. Feng, and L. Jiang, Adv. Funct. Mater. **18**, 3219 (2008).
[13]M. J. Hancock, K. Sekeroglu, and M. C. Demirel, Adv. Funct. Mater. **22**, 2223 (2012).
[14]D. Wu, J. N. Wang, S. Z. Wu, Q. D. Chen, S. Zhao, H. Zhang, H. B. Sun, and L. Jiang, Adv. Funct. Mater. **21**, 2927 (2011).
[15]S.-G. Park, J. H. Moon, H. C. Jeon, and S.-M. Yang, Soft Matter **8**, 4567 (2012).
[16]J. Yong, Q. Yang, F. Chen, D. Zhang, U. Farooq, G. Du, and X. Hou, J. Mater. Chem. A **2**, 5499 (2014).
[17]S. Wang, K. Liu, X. Yao, and L. Jiang, Chem. Rev. **115**, 8230 (2015).
[18]A. R. Parker and C. R. Lawrence, Nature **414**, 33 (2001).
[19]W. Barthlott *et al*., Adv. Mater. **22**, 2325 (2010).
[20]C. A. Hamlett, N. J. Shirtcliffe, F. B. Pyatt, M. I. Newton, G. McHale, and K. Koch, Planta **234**, 1267 (2011).
[21]K. Liu, M. Cao, A. Fujishima, and L. Jiang, Chem. Rev. **114**, 10044 (2014).

[22]Y. Lai, J. Huang, Z. Cui, M. Ge, K. Q. Zhang, Z. Chen, and L. Chi, Small **12**, 2203 (2016).

[23]X. Zhang, M. Jin, Z. Liu, D. A. Tryk, S. Nishimoto, T. Murakami, and A. Fujishima, J. Phys. Chem. C **111**, 14521 (2007).

[24]S. Nishimoto et al., Appl. Surf. Sci. **255**, 6221 (2009).

[25]K. Tadanaga, J. Morinaga, A. Matsuda, and T. Minami, Chem. Mater. **12**, 590 (2000).

[26]X. Zhang, J. Zhang, Z. Ren, X. Zhang, T. Tian, Y. Wang, F. Dong, and B. Yang, Nanoscale **2**, 277 (2010).

[27]S. Lyu and W. Hwang, Appl. Phys. Lett. **107**, 201606 (2015).

[28]C.-F. Wang and T.-W. Hsueh, J. Phys. Chem. C **118**, 12399 (2014).

[29]S. M. Kang, I. You, W. K. Cho, H. K. Shon, T. G. Lee, I. S. Choi, J. M. Karp, and H. Lee, Angew. Chem. Int. Ed. **49**, 9401 (2010).

[30]X. Yang, X. Liu, Y. Lu, S. Zhou, M. Gao, J. Song, and W. Xu, Sci. Rep. **6**, 23985 (2016).

[31]X. Yang, X. Liu, Y. Lu, J. Song, S. Huang, S. Zhou, Z. Jin, and W. Xu, J. Phys. Chem. C **120**, 7233 (2016).

[32]H. Li, Y. Lai, J. Huang, Y. Tang, L. Yang, Z. Chen, K. Zhang, X. Wang, and L. P. Tan, J. Mater. Chem. B **3**, 342 (2015).

[33]T. Chen, H. Liu, H. Yang, W. Yan, W. Zhu, and H. Liu, RSC Adv. **6**, 43937 (2016).

[34]A. Cassie and S. Baxter, Trans. Faraday Soc. **40**, 546 (1944).

[35]C.-F. Wang, W.-Y. Chen, H.-Z. Cheng, and S.-L. Fu, J. Phys. Chem. C **114**, 15607 (2010).

[36]S. Moradi, S. Kamal, P. Englezos, and S. G. Hatzikiriakos, Nanotechnology **24**, 415302 (2013).

[37]B. Chichkov, C. Momma, S. Nolte, F. Von Alvensleben, and A. Tünnermann, Appl. Phys. A **63**, 109 (1996).

[38]M. Gubko, A. Ionin, S. Kudryashov, S. Makarov, A. Rudenko, L. Seleznev, and D. Sinitsyn, JETP Lett. **97**, 599 (2013).

[39]N. Bloembergen, IEEE. J. Quantum Electron. **10**, 375 (1974).

[40]D. Von der Linde, K. Sokolowski-Tinten, and J. Bialkowski, Appl. Surf. Sci. **109**, 1 (1997).

[41]J. Kido, H. Hayase, K. Hongawa, K. Nagai, and K. Okuyama, Appl. Phys. Lett. **65**, 2124 (1994).

[42]T. Monde, H. Fukube, F. Nemoto, T. Yoko, and T. Konakahara, J. Non-Cryst. Solids **246**, 54 (1999).

[43]R. N. Wenzel, J. Phys. Chem **53**, 1466 (1949).

[44]W. Choi, A. Tuteja, J. M. Mabry, R. E. Cohen, and G. H. McKinley, J. Colloid Interface Sci. **339**, 208 (2009).

[45]K. Li, J. Ju, Z. Xue, J. Ma, L. Feng, S. Gao, and L. Jiang, Nat. Commun. **4**, 2276 (2013).

[46]E. Mele, S. Girardo, and D. Pisignano, Langmuir **28**, 5312 (2012).

[47]J. Y. Chung, J. P. Youngblood, and C. M. Stafford, Soft Matter **3**, 1163 (2007).

[48]X. D. Zhao, H. M. Fan, X. Y. Liu, H. Pan, and H. Y. Xu, Langmuir **27**, 3224 (2011).

[49]H. Y. Erbil and C. E. Cansoy, Langmuir **25**, 14135 (2009).

[50]D. Zhang, F. Chen, Q. Yang, J. Si, and X. Hou, Soft Matter **7**, 8337 (2011).

[51]J. Y. Huang, Y. K. Lai, F. Pan, L. Yang, H. Wang, K. Q. Zhang, H. Fuchs, and L. F. Chi, Small **10**, 4865 (2014).

[52]Y. Lai, F. Pan, C. Xu, H. Fuchs, and L. Chi, Adv. Mater. **25**, 1682 (2013).

[53]A. Ghosh, R. Ganguly, T. M. Schutzius, and C. M. Megaridis, Lab Chip **14**, 1538 (2014).

[54]See supplementary material at http://dx.doi.org/10.1116/1.4966617 for rougness profile curves and SEM images of laser induced superhydrophobic surface.